Geochimica et Cosmochimica Acta 373 (2024) 98–108

Contents lists available at ScienceDirect

Geochimica et Cosmochimica Acta

journal homepage: www.elsevier.com/locate/gca

Characterising the decay of organic metal complexes in speleothem-forming cave waters

Sebastian N. Höpker [a,*], Sebastian F.M. Breitenbach [b], Megan Grainger [a], Claudine H. Stirling [c], Adam Hartland [a,d]

[a] Te Aka Mātuatua, School of Science, University of Waikato, Kirikiriroa Hamilton 3216, Aotearoa New Zealand
[b] Department of Geography and Environmental Sciences, Northumbria University, Newcastle upon Tyne NE7 7XA, United Kingdom
[c] Centre for Trace Element Analysis and Department of Geology, University of Otago, Dunedin 9054, Aotearoa New Zealand
[d] Lincoln Agritech Ltd, Ruakura, Kirikiriroa Hamilton 3214, Aotearoa New Zealand

ARTICLE INFO

Associate editor: Mélanie Davranche

Keywords:
Organic complexation
Competitive ligand exchange
Trace metal
Carbonate
Aqueous chemistry
Transition metal

ABSTRACT

Organic metal complexes (OMCs) transport trace metals (*e.g.*, Co, Ni, Cu) from surface soils, via the unsaturated zone, to sites of cave carbonate (speleothem) formation. OMCs clearly imprint on speleothem trace element chemistry, but the role of kinetic factors in the signal transfer process has yet to be elucidated. We investigated whether OMCs may viably link metal concentrations in stalagmites and local hydrology (*i.e.*, drip rate), via their time-sensitive dissociation (or 'decay') in the speleothem water thin-film. We performed competitive ligand exchange experiments using water and soil samples from eight geographically diverse Aotearoa New Zealand caves, providing a first comparative characterisation of speleothem-specific OMC kinetics. Critically, this approach corroborated that NOM ligands limit transition metal availability at the dripwater-speleothem interface, exhibiting stabilities on the order Cu ≈ Co > Ni, whereas organic complexation of the alkaline earth metals Mg and Sr was virtually absent. Systematic variations of OMC stability with natural organic matter characteristics were not observed amongst water samples, whilst enhanced complexation was clearly evident in the comparably organic-rich soil extracts. Our results imply that the supply of transition metals to speleothems is inversely related to drip rate, increasing with drip interval via the decay of OMCs. This process appears most sensitive on time-scales relevant to typical speleothem-forming settings (<0 to ca. 40 drips min^{-1}, corresponding to ca. <5.6 mL min^{-1}), and therefore provides a general, mechanistic link to a quantitative proxy of palaeoclimatic cave drip rates.

1. Introduction

The speciation, mobility, and bioavailability of trace metals in aquatic environments are tightly governed by interactions of metals with ligands present in natural organic matter (NOM) (Allen and Hansen, 1996; Sigg and Behra, 2005). At pH values of 8–9, typical for karst waters, NOM ligands generally bind >90 % of the total pool of Cu, Co, and Ni (*e.g.*, Hartland and Zitoun, 2018; Xue et al., 2000), thereby leaving only a marginal labile (available) fraction of hydrated 'free' cations and simple inorganic metal complexes (Hoffmann et al., 2007; Lead and Wilkinson, 2006). Consequently, organic metal complexes (OMCs) effectively control transition metal transport from the soil to caves (Hartland and Zitoun, 2018), where infiltrating waters deposit speleothems (secondary cave carbonates). In this process, fine colloidal particles (ca. <100 nm) and smaller nanoparticles (<1 nm) are understood to be particularly important (Hartland et al., 2011; Hartland et al., 2012), owing to their ability to be readily transported through the karst system, and their dominant relative abundance. NOM size classes typically follow a Pareto-like distribution, where the vast majority of particles measures around 1 nm or smaller (Doucet et al., 2007; Filella and Buffle, 1993; Hartland et al., 2011). Moreover, the potential for complexation within the smaller size fractions of NOM is generally enhanced, presumably due to a greater specific surface area compared to coarse colloids (>100 nm) or particulates (>1000 nm) (Buffle et al., 1998). Although larger organic compounds likewise host abundant ligands, their typically reduced mobility and more hydrophobic chemical structure tend to favour their deposition prior to reaching the cave during low flow regimes, or their direct entrapment or adsorption to

* Corresponding author.
E-mail address: sebastian.hoepker@waikato.ac.nz (S.N. Höpker).

https://doi.org/10.1016/j.gca.2024.03.024
Received 5 October 2023; Accepted 25 March 2024
Available online 27 March 2024

speleothem surfaces as undissociated complexes (*e.g.*, Borsato et al., 2007). While such accumulation of organic inclusions and associated metals in speleothems is often interpreted to reflect strong discharge events (Borsato et al., 2007; Warken et al., 2022), we focus on a mechanistically distinct, and arguably perpetual hydrological sensitivity of transition metals associated with the nominally dissolved fraction (here defined as <0.45 μm) of colloidal and nano-scale OMCs.

The kinetic inhibition of transition metals imposed by organic ligands complicates the apparent partitioning between dripwater and speleothems (estimated as the ratio of $(M/Ca)_{solid}$ and $(M/Ca)_{solution}$, where M and Ca are concentrations of a transition metal and calcium, respectively) (Lindeman et al., 2022). This stands in contrast to alkaline earth metals (*e.g.*, Mg, Sr, Ba), which exhibit comparably predictable partitioning that allows these elements to routinely serve as palaeoenvironmental proxies in speleothems (*e.g.*, Fairchild and Treble, 2009; Huang and Fairchild, 2001; Wassenburg et al., 2020). As exemplified for Cu, the 'aqueous sink' for transition metals created by organic complexation effectively moderates their availability for substitution into Ca^{2+} sites in the calcite lattice at the dripwater-calcite interface. Thus, the dissociation, or 'decay', of OMCs is expected to determine respective metal concentrations in the speleothem (Hartland and Zitoun, 2018; Sliwinski et al., 2022). Considering that the residence time of the thin water film on top of a stalagmite is largely governed by the rate of incoming drips, a systematic understanding of OMC dissociation kinetics may offer an opportunity to quantitatively relate stalagmite metal concentrations to drip rate. The interactions between a metal M and a ligand L_i are defined by the equilibrium describing the formation and dissociation of ML complexes (*i.e.*, OMCs; Equation (1)):

$$M + L_i \underset{k_{f,i}}{\overset{k_{d,i}}{\rightleftharpoons}} ML_i, \tag{1}$$

where the dissociation rate constant ($k_{d,i}$) is proportionate to the ratio of the formation rate constant ($k_{f,i}$) and the stability constant K of the equilibrium reaction for a given ligand (Equation (2)):

$$k_{d,i} = \frac{k_{f,i}}{K_i} \tag{2}$$

For the quantitative analysis of dissociation kinetics, the concentration of metal–ligand complexes in solution over time is commonly described in terms of an exponential decay with k_d as the rate-determining variable. To best account for the large number of heterogeneous binding sites in NOM (Rate et al., 1992), the total concentration of a metal due to dissociation at any given time t (C_t) can be expressed as a function of a continuous distribution of k_d (opposed to discrete values) (Equation (3)):

$$C_t = C^0 \int_{-4\sigma}^{+4\sigma} f(\ln k_d) \times e^{(-k_d \times t)} d(\ln k_d), \tag{3}$$

where C_0 denotes the initial metal concentration, and $f(\ln(k_d))$ describes the normal distribution of $\ln(k_d)$ with mean μ and standard deviation σ (Equation S5; see details in the Supplementary Material). One approach to study complex dissociation kinetics is the competitive ligand exchange (CLE) method, in which dissociation is induced by the introduction of a competing, typically very strong and well-characterised ligand to a test solution (*e.g.*, Chakrabarti et al., 1994; Sigg et al., 2006). Due to this competition, the equilibrium in Equation (1) favours the formation of metal complexes with the introduced ligand, in turn driving the decay of native OMCs. Rate constants describing this process can be estimated by monitoring the removal of metals from the sample solution over time.

In this study, we provide a set of quantitative estimates of OMC dissociation rate constants (k_d) for Ni, Cu, and Co in waters and soil extracts from eight Aotearoa New Zealand (from here, Aotearoa) caves via CLE experiments and kinetic modelling. Based on this information, we aim to elaborate on the hypothesis of a hydrological control of the concentrations of these metals in cave waters and speleothems as proposed by Hartland and Zitoun (2018), and move towards extracting meaningful and well-constrained palaeoenvironmental information from these.

2. Materials and methods

2.1. Sample solutions

Test solutions for kinetic experiments were obtained from eight Aotearoa cave systems with various soil and vegetation cover, and distinct climatic regimes (see Table S2 for details). Cave water samples were collected by placing acid-clean screw-cap Nalgene© high-density polyethylene (HDPE) bottles directly under drip points (n = 7) or sampling stream water (n = 1). After transfer to the laboratory, samples were filtered (0.45 μm) and stored frozen in the dark until analysis, while sub-samples were used for the determination of basic indices of NOM properties (see Section S2 of the Supplementary Material for details). Remote sampling locations and/or shipment of some samples prevented consistent pre-treatment, but analyses were carried out within three weeks of sample collection. By filtering the samples prior to experiments, we aimed to remove larger particles, targeting primarily the 'dissolved' fraction of smaller colloids and nanoparticles that are understood to contribute most of the kinetic behaviour operating at speleothem surfaces (Hartland et al., 2011). Native concentrations of transition metals in cave waters are typically close to instrumental quantitation limits (often <0.1 μg L^{-1} for Ni, Cu, Co), rendering the study of dissociation kinetics in untreated samples analytically challenging. Defrosted cave waters were therefore augmented with 5 μg L^{-1} of Ni, Cu, and Co to facilitate quantification of these elements, a tactic previously employed in several comparable experiments (*e.g.*, Lam et al., 1999; Mandal et al., 1999; Miller et al., 2012). Metal spikes were added by volume using analytical pipettes, which were calibrated gravimetrically (varying by <2 %) prior to the series of experiments. The same batch of elemental stock solutions was used for all test solutions. For a 400 mL volume of test solution as used here, we assume an uncertainty in total volume of ±2.5 mL (quoted uncertainty of graduated cylinders used to measure out test solutions). Based on these uncertainties and a conservative estimate of propagated errors of 5 % associated with the preparation of elemental stock solutions, we attribute a maximal deviation of <8 % in added transition metal concentration from the target of 5 μg L^{-1}. From three of the studied caves (Table 1), representative soil samples from ca. 10 cm depth were dried at 40 °C for 48 h, manually homogenised, and finally sieved (2 mm). Soil extracts were prepared by shaking soil sub-samples at a 1:10 (weight/volume) ratio in 0.01 M $CaCl_2$ for 2 h, followed by centrifuging for 10 min at ca. 1810 *g*, and finally filtering the supernatant (0.45 μm). 400 mL of the soil extracts and cave waters (spiked with transition metals) were adjusted to a concentration of 0.005 M HEPES buffer (N-hydroxyethylpiperazine-N'-2'-ethanesulphonic acid) and a pH of 8.5 to facilitate direct comparison of kinetic parameters. The selection of the buffer was based on a compromise between its metal complexation properties and pH range being representative of *in-situ* values (Ferreira et al., 2015). Although some measurable complexation of Cu by ligands present in the HEPES buffer solution has been reported (*e.g.*, Mash et al., 2002), this effect is assumed to be small in relation to complexation by natural ligands. Further, this effect is expected to be of the same magnitude in all experiments. The experimental pH of 8.5 was chosen based on the median of all dripwater samples (pH 8.52), which varied between pH 8.25 and pH 8.70 *in-situ*. Similarly, 3 M KCl was used to adjust the ionic strength of cave water solutions to ca. 0.018 M, whereas soil extracts were measured at their original ionic strength of ca. 0.044 M (HC-Soil and MAJ-Soil) and 0.087 M (Babylon-Soil). While the *in-situ* ionic strength (derived from measurements of electrical conductivity) of water samples was between 0.005 M and 0.008 M (291–509 μS cm^{-1}), the adjustment accounted for added ions during pH buffering to create comparable

Table 1
Overview of CLE test solutions and experimental conditions. Dissolved organic carbon (DOC), indicative parameters of NOM quality, and native metal concentrations were determined using filtered (0.45 μm) aliquots of otherwise unaltered water samples and $CaCl_2$ soil extracts. Uncertainties for metal concentrations reflect 1 standard deviation (SD) of triplicate measurements. DL refers to the respective instrumental detection limit.

Test solution	Experimental conditions			Selected properties of untreated test solutions								
	pH	Ionic strength	Temp.	DOC	$SUVA_{254}$	E_3/E_4	S_R	[Co]	[Ni]	[Cu]	[Mg]	[Sr]
	Median	mol L^{-1}	average, °C	mg L^{-1}	L mg^{-1} m^{-1}	a(300)/a(400)		μg L^{-1}	μg L^{-1}	μg L^{-1}	μg L^{-1}	μg L^{-1}
Cave waters												
Babylon Cave	8.48	0.016	22.3	2.1	153.5	2.17	2.91	<DL	<DL	0.099 ± 0.020	1560 ± 78	39.1 ± 2.0
Bulmer Cave	8.53	0.017	22.5	4.8	29.3	0.08	0.62	<DL	<DL	0.145 ± 0.029	1120 ± 56	24.6 ± 1.2
Calcite Cave	8.48	0.019	22.2	1.4	116.2	0.13	0.67	0.005 ± 0.001	<DL	0.178 ± 0.038	1340 ± 67	63.5 ± 3.2
Dave's Cave	8.48	0.017	22.2	2.9	161.6	0.15	0.40	0.007 ± 0.001	<DL	<DL	40 ± 2	2.0 ± 0.1
Hodge Creek Cave	8.46	0.019	22.1	4.1	197.4	0.70	1.01	0.010 ± 0.002	<DL	0.190 ± 0.038	1210 ± 61	77.4 ± 3.9
Majumba Cave	8.53	0.023	21.7	6.8	85.1	1.49	0.44	0.009 ± 0.002	0.077 ± 0.015	0.210 ± 0.042	5340 ± 270	365.0 ± 18.0
Stafford's Cave (stream)	8.49	0.016	21.9	2.5	325.7	0.49	1.20	<DL	0.276 ± 0.028	0.076 ± 0.015	1160 ± 58	77.7 ± 3.9
Te Reinga Cave	8.54	0.017	22.3	2.9	194.1	0.34	0.90	<DL	0.064 ± 0.013	0.078 ± 0.016	2250 ± 110	340.0 ± 17.0
All water experiments	8.49	0.018 ± 0.002	22.1 ± 0.3									
Soil extracts												
Babylon Cave	8.50	0.087	22.4	60.5	540.8	6.78	0.96	0.337 ± 0.017	2.816 ± 0.142	7.014 ± 0.351	76238 ± 3811	1108.0 ± 55.9
Hodge Creek Cave	8.45	0.043	22.5	17.9	331.5	3.37	1.36	0.068 ± 0.014	0.937 ± 0.187	6.181 ± 0.309	7650 ± 385	499.5 ± 24.8
Majumba Cave	8.48	0.044	21.7	9.2	651.8	2.95	1.06	0.089 ± 0.018	1.055 ± 0.209	4.193 ± 0.209	20939 ± 1070	754.0 ± 37.7
All soil extract experiments	8.48	0.058 ± 0.025	22.2 ± 0.4									

conditions between experiments. *In-situ* water temperatures (between 6.8 °C and 15.9 °C) were not attempted to be replicated here but are expected to be of minor importance (Rieuwerts et al., 1998). Since native metal concentrations varied only slightly between water samples with all three transition metals of interest having natural concentrations near instrumental detection limits (Table 1), the addition of 5 μg L^{-1} of each element is regarded to affect all aqueous samples equally. Treated test solutions were stirred in the dark in sealed acid-cleaned 1000 mL Nalgene© HDPE bottles that served as reactors, and were allowed to equilibrate at experimental temperature for 24 h prior to the experiment.

2.2. Competitive ligand exchange experiments

M-NOM decay kinetics were studied via competitive ligand exchange experiments, which we consider suitable given established application in kinetic studies, and comparably limited dependence on specialised equipment. In these experiments, the decay of natural OMCs in the test solutions is induced by introducing a well-characterised, strong ligand (typically a wet ion exchange resin), which attracts and binds nearby ions. The latter include originally labile ('free') metal cations and those freshly released from decaying complexes, which in turn remain in solution. The rate of OMC decay is quantified by monitoring the concentration of metals measured in the test solution (*i.e.*, cations not bound by the resin) as a function of time, thus reflecting the metal fraction that remains complexed by natural ligands. Due to a fundamental variability in binding properties of different ligands and metals, and their sensitivity to the solution characteristics (*e.g.*, pH, ionic content), however, it is important to note that derived kinetic parameters are inevitably specific to the experimental conditions.

In this study, Chelex® 100 ion exchange resin (Bio-Rad Laboratories, Inc., USA; Na-form, 200–400 mesh; herein Chelex-100) was selected as the competing ligand to bind metal cations due to its wide use in similar ligand exchange experiments, as well as in alternative approaches used to constrain complex dissociation kinetics (*e.g.*, using diffusive gradients in thin-films; Levy et al., 2012; Shafaei Arvajeh et al., 2013). Since Chelex-100 in Na-form has a pH of ca. 10–11 in water, the resin was pre-conditioned prior to the experiments to prevent significant disruptions to the desired experimental solution pH. To this effect, Chelex-100 was initially suspended in an excess volume of 0.1 M HEPES buffer solution (adjusted to pH 8.5 with 1 M or 0.1 M NaOH) for at least 24 h in the dark using a Teflon-coated magnetic stir bar to stabilise the pH of the resin to that of the test solutions. Prior to the pH equilibration of the resin, the buffer solution was purified by stirring 5 % Chelex-100 (weight/volume) for 12 h, and subsequently removing and discarding the resin by filtration (0.45 μm). The pre-conditioned resin was extracted shortly before each experiment by centrifuging the mixture for 20 min at ca. 1810 *g*, and subsequently extracting the supernatant buffer solution. Each experiment was initiated with the addition of 1 % (wet weight/volume; *i.e.*, 4 g for 400 mL solution) of pre-treated resin to the stirred test solution. Including one sub-sample collected just prior to the start of the experiment, a total of 12 aliquots were taken at intervals evenly distributed in log-space ranging from 10 s to 7200 s following Chelex-100 addition. This duration of the kinetic experiments was determined based on results from reconnaissance experiments under equivalent conditions, which indicated little to no change in the undissociated fraction over 72 h. The sub-samples were drawn from the reactor and immediately filtered using syringes equipped with 0.45 μm PES filters and Tygon® Inert tubing, thus separating the sub-sample of test solution from the Chelex-100 resin. Accordingly, any metal cations present in the filtered sub-sample is considered to reflect the fraction of undissociated OMCs at the respective time. Aliquots of these sub-samples were immediately acidified to 2 % (volume/volume) with double-distilled HNO_3 for the analysis of elemental concentrations by inductively-

coupled plasma mass spectrometry (ICP-MS). Assuming that there is no significant aggregation of NOM during the experiments, we do not expect the filtration to cause additional size fractionation. The solution pH across all experiments was maintained at 8.5 and varied by less than 0.3 pH units over the duration of individual experiments. Solution temperature was kept at 22.2 °C ± 0.3, with an ionic strength of 0.018 M ± 0.002 for water samples (variable for soil extracts). An overview of experiments and information on test solutions is presented in Table 1. Details on chemical analyses are found in Section S2 of the Supplementary Material.

2.3. Kinetic data analysis

Continuous distributions of conditional dissociation rate constants (k_d) for each CLE experiment were estimated based on the measured total metal concentrations normalised to respective initial concentrations (*i.e.*, C_t/C_0). This was achieved by numerically integrating Equation (3) and subsequently fitting μ and σ in $f(\ln(k_d))$ (see Equation S5) as proposed by Rate et al. (1992), where μ and σ reflect the mean and standard deviation of a normal distribution of $\ln(k_d)$, respectively. The same datasets were also fitted to discrete site models. Details on both modelling approaches are found in the Supplementary Material (Section S2.7).

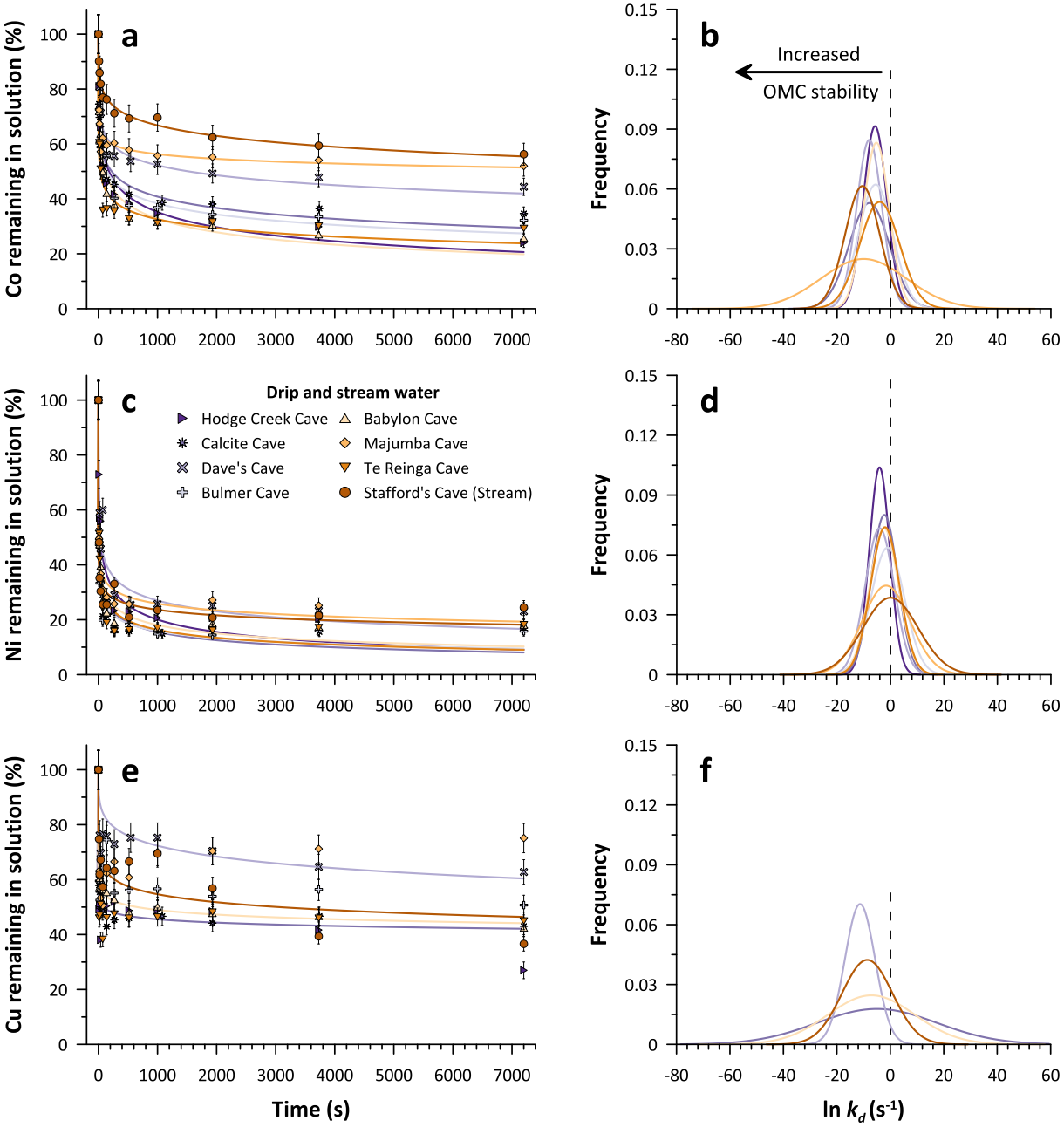

Fig. 1. OMC decay curves and corresponding fitted log-normal distributions of k_d for transition metals in CLE experiments of cave waters. Sub-figures **a**, **c**, and **e** show the measured evolution of metal concentrations in solution (symbols) and corresponding log-normal model fits (solid lines) according to Equation (3) (Rate et al., 1992). Vertical error bars denote propagated standard deviations (1 SD). The right column (sub-figures **b**, **d**, **f**) contains the respective frequency distributions (site densities) of $\ln(k_d)$ based on fitted values of μ and σ. Note that fitted values for σ produce excessively large distributions of $\ln(k_d)$. Where only symbols are shown, no adequate model fit was obtained. Values of $\ln(k_d) > -2$ cannot accurately be distinguished from the decay of metal-aqua complexes.

3. Results

3.1. Chemical properties of unaltered cave water and soil solutions

The transition metals of interest were consistently low in concentrations, with Co, Ni, and Cu varying between unquantifiable contents and ca. 0.01 μg L^{-1}, 0.28 μg L^{-1}, and 0.21 μg L^{-1}, respectively (Table 1). Mg and Sr concentrations ranged from 40 μg L^{-1} to 5340 μg L^{-1}, and 2 μg L^{-1} to 365 μg L^{-1}, respectively, with the by far lowest values corresponding to the alpine Dave's Cave. The dissolved organic carbon (DOC) content varied between 1.4 mg L^{-1} and 6.8 mg L^{-1}, and was highest in Majumba Cave. Indices of NOM properties suggested that organic components in all water samples were dominated by humic acids with a relatively high degree of humification (see Fig. S1a). Native transition metal concentrations generally scaled positively with DOC content (Fig. S1b) but other relationships amongst organic indices and elemental measurements were not discernible.

In soil extracts, native transition metal concentrations ranged from 0.07 μg L^{-1} to 0.34 μg L^{-1} (Co), 0.94 μg L^{-1} to 2.82 μg L^{-1} (Ni), and 4.19 μg L^{-1} to 7.01 μg L^{-1} (Cu). There was a ten-fold difference between the Mg content of soils from Hodge Creek Cave (ca. 7.65 mg L^{-1}) and Babylon Cave (ca. 76.24 mg L^{-1}), while Sr in soil extracts varied by a factor of ca. 2 (500–1108 μg L^{-1}). The DOC content of soil extracts was consistently much higher than in any water sample (9.2–60.5 mg L^{-1}), although relative magnitudes in DOC concentrations between the two media were seemingly unrelated. Compared to water samples, all three soil extracts showed a lower degree of humification, while soil from Babylon Cave was the only sample likely dominated by fulvic acid components (Fig. S1a).

3.2. Kinetic characterisation of OMC decay

Initial transition metal concentrations in water solutions generally decreased exponentially upon Chelex-100 addition, with most of the OMC decay occurring within the first ca. 15 min of each CLE experiment (Fig. 1). A fraction of transition metals remaining undissociated from complexes after two hours (referred to here as the 'inert' fraction, or % M_{2h}) was observed in all experiments, specifically 30–60 % (Co), 15–25 % (Ni), and 30–80 % (Cu) (Table 2). Estimates of the mean μ of the normal distribution of $\ln(k_d)$ in cave waters varied between ca. -1.1 s^{-1} and -8.3 s^{-1} ($k_d = 3.3\times10^{-1} - 2.5\times10^{-4}$ s^{-1}) for Ni, and between -4.1 s^{-1} and -10.5 s^{-1} ($k_d = 1.7\times10^{-2} - 2.8\times10^{-5}$ s^{-1}) for Co (Table 2, Fig. 1). For Cu, three adequate models yielded values of μ between ca. -5.0 s^{-1} and -8.6 s^{-1} ($k_d = 8.5\times10^{-4} - 6.9\times10^{-3}$ s^{-1}). Inconsistent variations in Cu concentrations over time (*i.e.*, no monotonous decrease) prevented model fits in the remaining experiments. Fitted values of σ (the standard deviation of the normal distribution of $\ln(k_d)$) ranged from 3.8 to 22.5 across transition metal models, with the largest values corresponding to the three Cu models. The continuous models thereby consistently describe a substantial range of k_d around the respective log-normal distribution's mean μ, whilst also highlighting considerable variability in OMC stabilities between sample solutions, as well as between different transition metals. Of the latter, the most consistent kinetic behaviour was exhibited by Ni, while overall OMC stability was approximately in the order of Cu ≈ Co > Ni (Fig. 2). Discrete models (solved for one to three terms) generally yielded the best fits assuming two or three kinetic components. In most cases, the dominant resolved kinetic component accounted for ca. 40–87 % and was typically associated with a fitted k_d in the same order of respective estimates of μ. Additional kinetic components varied highly in k_d (by up to 5 orders in

Table 2
OMC decay characteristics for transition metals in cave waters and soil extracts determined in CLE experiments. Values of μ and σ were fitted using the continuous (log-normal) kinetic model described by Rate et al. (1992) (Equation (3). The discrete model is described in Equation S4 and was solved for 1–3 kinetic components (*i.e.*, C_1, C_2, C_3, expressed as percentages) with corresponding dissociation rate constants. $\%M_{2h}$ denotes the fraction of OMCs that remained undissociated after two hours. Data are only shown where adequate model fits were obtainable ($R^2 > 0.75$). The threshold k_d (τ^{-1}) was 1.4×10^{-4} s^{-1} for all transition metal fits. Kinetic parameters obtained for Mg and Sr are found in Supplementary Table S1.

		Continuous kinetic model				Discrete kinetic model							$\%M_{2h}$
		$\mu \pm 1$ SD $\ln(k_d)$	$\sigma \pm 1$ SD $\ln(k_d)$	k_d s^{-1}	R^2	C_1 %	C_2 %	C_3 %	$k_{d,1}$ s^{-1}	$k_{d,2}$ s^{-1}	$k_{d,3}$ s^{-1}	R^2	
Cave waters													
Ni	Babylon Cave	−2.4 ± 0.5	5.4 ± 0.9	9.2×10^{-2}	0.96	42.3	39.8	17.9	2.5	1.8×10^{-2}	6.2×10^{-7}	1.00	18.0
	Bulmer Cave	−1.1 ± 0.8	6.3 ± 1.1	3.4×10^{-1}	0.96	60.7	23.1	16.2	1.8×10^{-1}	1.5×10^{-2}	6.2×10^{-6}	0.99	15.8
	Calcite Cave	−2.3 ± 0.6	5.00 ± 0.9	1.0×10^{-1}	0.95	78.1	19.0		6.2×10^{-2}	3.2×10^{-5}		0.97	17.1
	Dave's Cave	−4.1 ± 0.6	5.4 ± 1.3	1.7×10^{-2}	0.90	86.9	25.6	6.5	2.6×10^{-2}	1.6×10^{-5}	4.1×10^{-3}	0.75	23.0
	Hodge Creek Cave	−4.1 ± 0.4	3.8 ± 0.7	1.6×10^{-2}	0.92	57.7	22.6	19.8	2.1×10^{-2}	3.7×10^{-5}	2.1×10^{-1}	0.99	17.1
	Majumba Cave	−1.6 ± 0.8	8.9 ± 1.7	2.0×10^{-1}	0.96	42.1	32.0	25.8	2.2	2.5×10^{-2}	7.8×10^{-6}	1.00	24.2
	Stafford's Cave (stream)	No model				73.8	26.0		1.1×10^{-1}	2.5×10^{-5}		0.98	24.5
	Te Reinga Cave	−2.1 ± 0.7	5.4 ± 1.1	1.3×10^{-1}	0.94	79.8	18.4		5.6×10^{-2}	1.1×10^{-5}		0.98	18.2
Co	Babylon Cave	−5.3 ± 0.2	4.8 ± 0.5	5.1×10^{-3}	0.97	42.9	33.8	23.3	1.2×10^{-2}	4.5×10^{-5}	2.3	1.00	25.7
	Bulmer Cave	−5.6 ± 0.2	6.4 ± 0.8	3.9×10^{-3}	0.96	40.5	35.6	24.1	1.1×10^{-1}	1.4×10^{-5}	4.1×10^{-3}	0.98	32.2
	Calcite Cave	−6.0 ± 0.2	6.3 ± 0.7	2.5×10^{-3}	0.96	42.2	37.2	20.6	3.2×10^{-5}	1.7×10^{-2}	3.1×10^{-1}	0.99	34.6
	Dave's Cave	−7.9 ± 0.3	7.5 ± 1.2	3.6×10^{-4}	0.93	57.8	53.8		2.6×10^{-2}	2.9×10^{-5}		0.87	44.4
	Hodge Creek Cave	−5.8 ± 0.2	4.4 ± 0.4	3.1×10^{-3}	0.96	42.9	39.2	17.9	1.4×10^{-2}	7.3×10^{-5}	1.4×10^{-1}	1.00	24.0
	Majumba Cave	−10.0 ± 0.8	16.0 ± 2.8	4.4×10^{-5}	0.96	59.1	40.7		2.1×10^{-5}	1.0×10^{-1}		0.98	52.0
	Stafford's Cave (stream)	−10.5 ± 0.2	6.5 ± 0.5	2.7×10^{-5}	0.98	62.1	22.8	14.5	1.4×10^{-5}	4.4×10^{-2}	8.8×10^{-4}	0.99	56.2
	Te Reinga Cave	−4.1 ± 0.5	7.5 ± 1.3	1.7×10^{-2}	0.94	62.9	34.7		4.8×10^{-2}	3.0×10^{-5}		0.97	29.2
Cu	Babylon Cave	−7.1 ± 0.2	16.2 ± 1.7	8.5×10^{-4}	0.99	49.9	40.8	9.3	2.2×10^{-5}	2.6	4.7×10^{-3}	0.99	42.4
	Calcite Cave	−5.0 ± 0.6	22.5 ± 5.5	6.9×10^{-3}	0.97	45.5	37.3	17.2	4.6×10^{-6}	3.1	3.1×10^{-2}	0.99	43.0
	Stafford's Cave (stream)	−8.6 ± 0.9	9.4 ± 2.9	1.8×10^{-4}	0.77	65.4	23.9	10.9	8.8×10^{-5}	1.6×10^{-1}	1.6×10^{-1}	0.91	36.6
Soil extracts													
Ni	Babylon Cave	−8.3 ± 0.2	5.0 ± 0.6	2.5×10^{-4}	0.95	45.8	33.8	20.0	8.9×10^{-18}	2.5×10^{-2}	9.1×10^{-4}	0.99	46.5
Cu	Babylon Cave	−11.7 ± 0.3	5.5 ± 0.8	8.0×10^{-6}	0.96	75.2	16.4	8.4	3.1×10^{-5}	3.3×10^{-3}	9.3×10^{-2}	0.98	61.5
	Hodge Creek Cave	−11.0 ± 0.4	4.9 ± 1.1	1.7×10^{-5}	0.90	74.8	22.5		4.7×10^{-5}	5.6×10^{-3}		0.96	55.0
	Majumba Cave	−10.0 ± 0.6	4.3 ± 1.0	4.7×10^{-5}	0.87	77.7	19.0		1.0×10^{-4}	5.9×10^{-3}		0.96	39.4

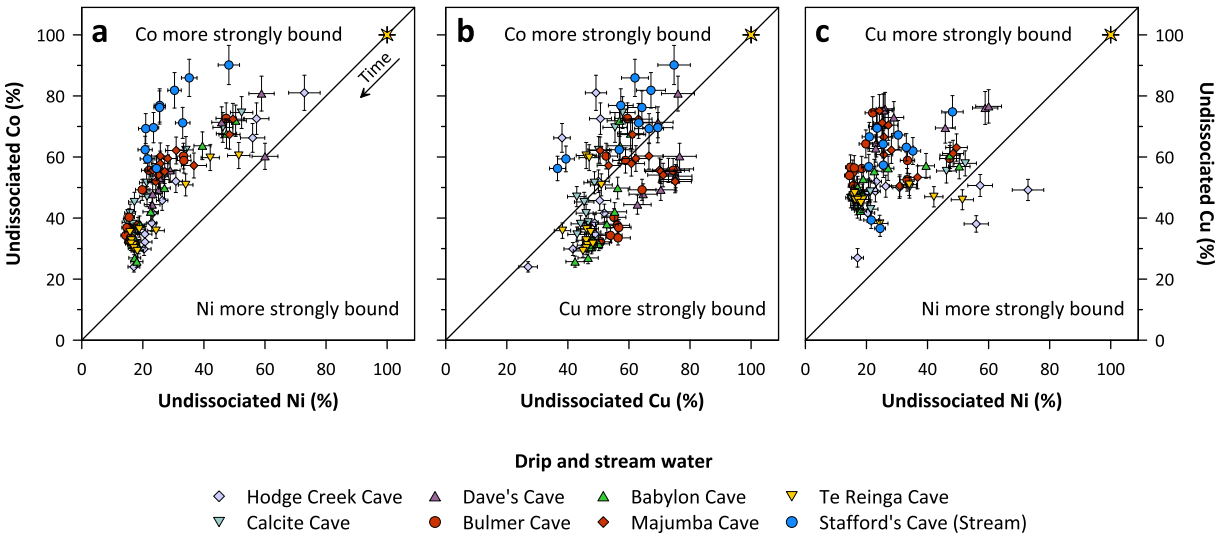

Fig. 2. Comparative transition metal fractions bound to OMCs over the course of CLE experiments. Organic complexes of Co and Cu consistently decayed more slowly than those of Ni but exhibited variable binding affinities between samples and with progressive dissociation. Error bars denote propagated standard deviations (1 SD) and for clarity are omitted for the common initial metal fraction of 100 % (yellow star symbol).

magnitude), suggesting the presence of both extremely labile and stable OMCs in the samples. Estimates of μ for Mg and Sr varied between -3.8 s^{-1} and -5.0 s^{-1} ($k_d = 2.4\times10^{-2} - 7.2\times10^{-3}$ s^{-1}), and -3.7 s^{-1} and -4.9 s^{-1} ($k_d = 2.2\times10^{-2} - 6.7\times10^{-3}$ s^{-1}), respectively, depicting very little variability between sample solutions (Table S1, Fig. 3). Less than 2 % of initial Mg and Sr were measured in test solutions at the end of all experiments, while the final Mg content in several experiments was not quantifiable. Rapid uptake of Mg and Sr by Chelex-100 was similarly evident in discrete models, which attributed ca. 50–84 % of the data fit to one kinetic component with similar values for k_d as respective estimates of μ (Table S1). There were no distinguishable relationships between derived kinetic parameters of the studied metals (both continuous and discrete model fits) and any of the indices used to assess NOM (Fig. S1).

For soil extracts, only three Cu models and one Ni model yielded adequate kinetic descriptions of the observations, while measurements of Co and Ni (for samples from Hodge Creek Cave and Majumba Cave) returned insufficient reliable data for fits to be calculated (Table 2). With μ varying between ca. -10.0 s^{-1} and -11.7 s^{-1} for Cu, and estimated as ca. -8.3 s^{-1} for Ni, soil-derived OMCs altogether appeared more stable than those in cave waters. This coincided with generally larger fractions of initial metal content in soil solutions remaining complexed after 2 h compared to water samples (ca. 39–61 % for Cu, 32–60 % for Ni), which was particularly pronounced for Co (80–91 %).

4. Discussion

4.1. Kinetic signatures of OMC decay in cave water and soil solutions

OMC dissociation kinetics for Ni, Co, and Cu in typical cave environments were characterised using dissociation rate constants (k_d) estimated for eight cave water samples and three soil extracts from Aotearoa via CLE experiments. An exponential decay of OMCs as commonly assumed was universally evident but distinct between different metals and samples. Estimates of the mean μ for the normal distribution of $\ln(k_d)$ in cave waters translated to k_d values of ca. $3.3\times10^{-1} - 2.5\times10^{-4}$ s^{-1} and $1.7\times10^{-2} - 2.8\times10^{-5}$ s^{-1} for Ni and Co, respectively (Fig. 1), suggesting an overall stronger kinetic limitation for Co. At the end of CLE experiments (*i.e.*, after 2 h), between 30 % and 60 % of initial Co remained undissociated in cave water solutions (denoted as $\%M_{2h}$), whereas only 15–25 % of Ni-NOM complexes persisted (Table 2). The tendency of Co to form more stable complexes coincided with a generally more heterogeneous kinetic behaviour. While distributions of $\ln(k_d)$ were comparably well constrained for Ni (*i.e.*, smaller fitted values of the distribution's standard deviation, σ), a larger range in k_d values was required to adequately describe the decay of Co-NOM complexes. However, the roughly asymptotic evolution of Ni and Co concentrations in most water samples after ca. 15 min of exposure to Chelex-100 attested to a relatively large proportion of both metals occupying weaker NOM binding sites. Although the latter may be exaggerated in this study due to procedurally increased M:NOM ratios by elemental spiking, a release of up to ca. 80 % and 64 % of Ni and Co was observed within ca. 2 min, respectively. The average k_d (4.0×10^{-3} s^{-1} as derived from fitted μ) for Co-NOM was highly comparable to that found by Warnken et al. (2007) in stream waters at a comparable pH ≈ 8 (3.1×10^{-3} s^{-1}), whereas Ni-NOM dissociation rate constants in their study (6.6×10^{-4} s^{-1}) suggested considerably more stable complexation than implied here by an average k_d for Ni-NOM of 1.1×10^{-1} s^{-1}. Ni dissociation curves in turn compared well with those for a Ni:Fa of 0.25 and pH 7.6 modelled by Shi et al. (2016), who compiled CLE experimental data from various previous studies (Fa representing fulvic acid).

The kinetic behaviour of Cu was less distinct, with several experiments exhibiting an unexpected increase in dissolved Cu following its initial rapid uptake by the Chelex-100 resin. Despite pre-conditioning containers, this may be due to desorption from the reactor walls, or alternatively be linked to more intricate processes and interactions with other metals at the binding sites of NOM ligands (*e.g.*, site competition; Mandal et al., 1999). Regardless, while showing an overall exponential decay (as expected) the complicated behaviour immediately after experiment initiation precluded adequate kinetic models for most samples. Fits yielded values of μ translating to k_d in the order of $9\times10^{-4} - 7\times10^{-3}$ s^{-1}, while between 30 % and 80 % of initial Cu remained undissociated. This magnitude of k_d for Cu-NOM complexes is similar to that reported by Warnken et al. (2007) (ca. 6.1×10^{-2} s^{-1}), while reflecting lower complex stability than in solutions with known anthropogenic contributions (see Baken et al. (2011), but not Amery et al. (2010)). Based on fitted values of μ (Table 2) and an assessment of comparative metal binding throughout experiments (Fig. 2), the data thus depict a stronger binding affinity of Cu and Co to NOM than Ni across cave water samples, which is partly at odds with the predicted hierarchy of Cu > Ni > Co according to the Irving-Williams series (Irving and Williams, 1953). However, these findings are in turn supported by

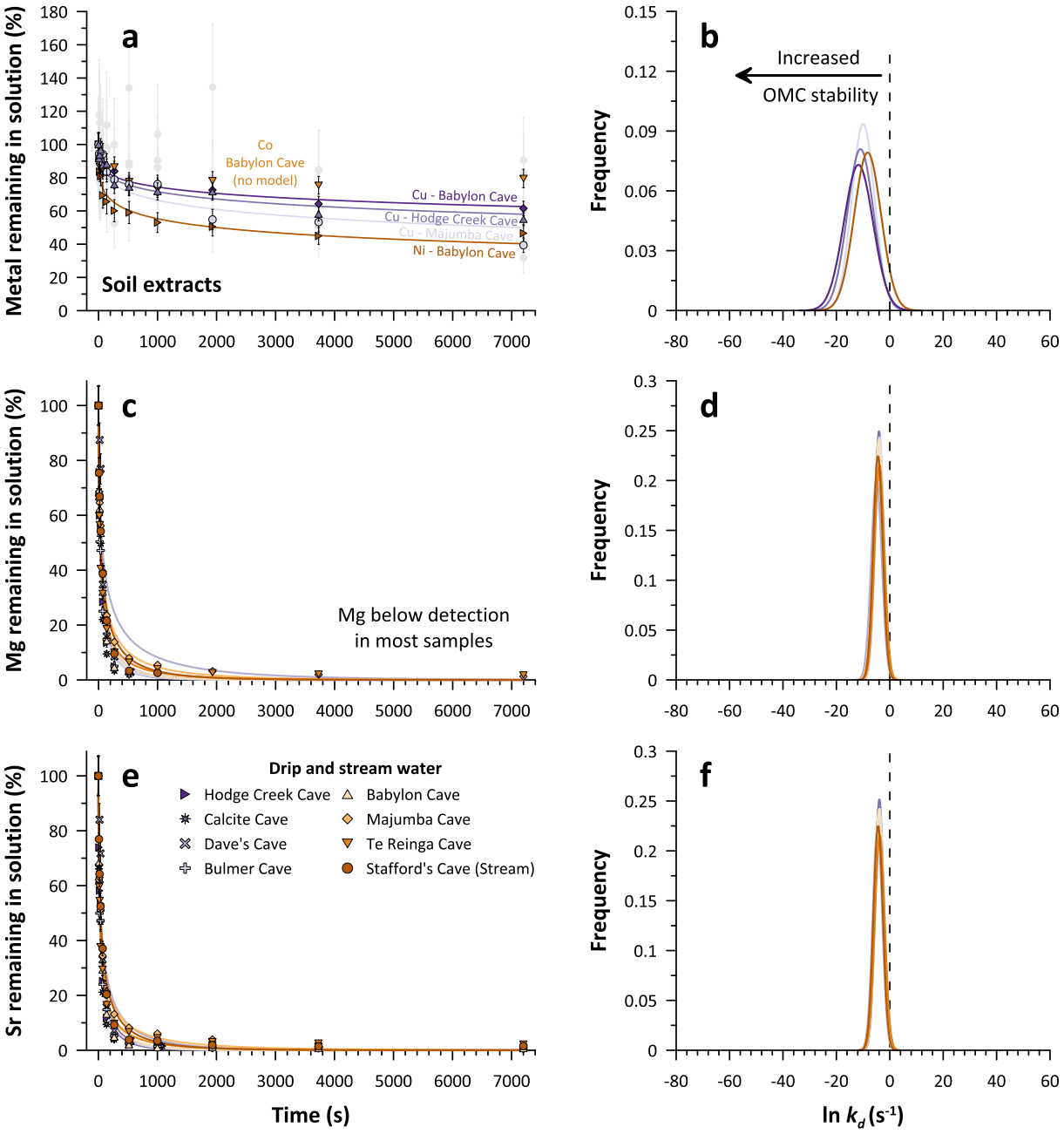

Fig. 3. OMC decay curves and corresponding fitted log-normal distributions of k_d for metals in CLE experiments of cave waters and soil extracts. Sub-figures **a**, **c**, and **e** show the measured evolution of metal concentrations in solution (symbols) and corresponding log-normal model fits (solid lines) according to Equation (3) (Rate et al., 1992). Vertical error bars denote propagated standard deviations (1 SD). The right column (sub-figures **b**, **d**, and **f**) depicts the respective frequency distributions (site densities) of $\ln(k_d)$ based on fitted values of μ and σ. Note that fitted values for σ produce excessively large distributions of $\ln(k_d)$. Where only symbols are shown, no adequate model fit was obtained. For clarity, the highly inconsistent measurements of Ni and Co in Majumba Cave and Hodge Creek Cave in sub-figure **a** are shown as light grey symbols. Values of $\ln(k_d) > -2$ cannot accurately be distinguished from the decay of metal-aqua complexes.

observations of Collins and Kinsela (2010) and Hartland et al. (2011), who reported exceedingly stable complexation of Co in natural freshwater systems.

Mg and Sr present the most widely assessed trace elements in speleothems and other carbonate archives. Here, both metals were readily removed from solution upon Chelex-100 addition to near or below detection limit in many water samples, with negligible fractions (<2.0 %) of initial concentrations remaining undissociated in the remaining experiments (Table S1). Despite a slowdown after ca. 3 min of the initially linear and rapid removal (Fig. 3), these results demonstrate the effective absence of strong ligand binding of Mg and Sr. Arguably, organic complexation is thus inconsequential to observed partitioning between dripwater and speleothems for these elements. Dissociation was highly consistent for Mg ($k_d = 2.4\times10^{-2} - 7.2\times10^{-3}$ s^{-1}) and Sr ($k_d = 2.2\times10^{-2} - 6.7\times10^{-3}$ s^{-1}) based on estimates of μ. The latter were strongly correlated between Mg and Sr ($r = 0.98$, $p < 0.0001$, n = 8), which was not the case for any other metal pairs. This may suggest that the source for the observed minimal kinetic limitation of Mg and Sr may be attributable to the HEPES buffer or equilibrium constraints rather than heterogeneous binding sites of natural organic ligands.

The stability of OMCs depends on several factors, the most determinant being pH, ionic strength, metal:ligand ratios, and the quality of ligands (*e.g.*, Sanders and Bloomfield, 1980; Rate et al., 1993). Empirically derived values of kinetic parameters are thus inherently

conditional and sensitive to the specific experimental design. One such methodological constraint for the quantitative interpretation of derived kinetic parameters is the analytical time-scale τ, which is defined by the experimental duration. Specifically, the duration of 2 h, during which OMC decay was monitored, imposes a threshold for the resolvable 'kinetic window' with limit τ^{-1} (Amery et al., 2010). For $\tau = 2$ h this translates to a threshold $k_d \approx 1.4\times10^{-4}$ s^{-1}, which may serve to operationally differentiate 'labile' and 'inert' fractions for $k_d > \tau^{-1}$ and $k_d < \tau^{-1}$, respectively. Accordingly, complexes thereby deemed 'labile' are expected to be mostly dissociated after 2 h, whereas 'inert' species remain largely complexed beyond the experimental duration (also reflected by $\%M_{2h}$). In case of the latter, k_d values are effectively extrapolated, limiting confidence in their absolute magnitude. A second limit exists as $t \rightarrow 0$. Adopting the threshold identified by Fasfous et al. (2004) for an equivalent kinetic window, decay constants of $k_d > 10^{-2}$ s^{-1} cannot reliably be attributed to OMCs because the fast dissociation rate approaches that of metal-aqua complexes. This limit further accounts for time required for the Chelex-100 to mix in solution. Interestingly, these constraints suggest that a considerable fraction of Ni was very weakly complexed, with fitted values of k_d indicating mostly 'labile' behaviour of most Ni complexes within the analytical time-frame. However, >20 % of Ni was persistently characterised as more stable and/or 'inert' in discrete models, which was also reflected by similar fractions of $\%Ni_{2h}$ (Table 2). On the other hand, Mg was not detectable beyond ca. 5–10 min of sub-sampling in most experiments, and $\%Sr_{2h}$ was consistently <2 %. Despite their fitted values of μ being comparable to those of transition metals, consideration of τ and the estimated proportions of kinetic components altogether depicts negligible or absent organic binding, which is largely indistinguishable from metal-aqua complexes.

Notwithstanding the caveats on absolute kinetic parameters, we primarily aimed to compare complexation characteristics of different cave waters representative of a range of environments. Regarding factors driving complex stability, the experimental pH of 8.5 was therefore selected to represent most limestone cave waters that typically vary in pH between 7.5 and 9. We note that significantly more alkaline systems with distinct complexation regimes are known (*e.g.*, Poole's Cavern; Hartland et al., 2011) but are an exception. Likewise, ionic strength was fixed but similar to that found in caves. Consequently, the observed variability in kinetic signatures is interpreted primarily as a function of ligand quality and quantity, which are expected to present the dominant variables driving OMC stability in common karst systems.

Following the interpretation of spectral absorption ratios (E_3/E_4) of Artinger et al. (2000), dissolved organic matter (DOM) in most samples was dominated by components resembling humic acid, as opposed to fulvic acid (Fig. S1a, Section S2 for details on methodology). On the other hand, clear trends were absent between samples with regards to molecular weight or aromaticity based on parameters derived from UV–Vis spectra, suggesting that DOM properties were not sufficiently distinct for such characterisations. Perhaps because of this, there was no pronounced relation between fitted values for $\ln(k_d)$ and DOC, nor between the former and the specific UV absorbance at 254 nm ($SUVA_{254}$) or other indices of NOM quality derived from UV–Vis spectra (all relationships $p > 0.05$; Fig. S1). These observations are coherent with a lack of correlation between ligand concentration and DOM content observed in dripwaters (Hartland and Zitoun, 2018) but contrast with several studies relating kinetic parameters to proxies of NOM properties. For instance, Amery et al. (2010) and Baken et al. (2011) noted a pronounced positive relationship of $SUVA_{254}$ with the fraction of non-labile Cu (undissociated after 8 h) and metal binding affinity (Ni, Cu, Co, Zn), respectively. Similarly, Welikala et al. (2018) observed that Ni in soil amendments was complexed more strongly by DOM of higher aromaticity (see also Baker et al., 2008). However, the discrepancies with many previously published datasets are not altogether surprising, given the often substantially greater metal and/or DOM contents and ranges of test solutions in other studies. For instance, natural stream water analysed *in-situ* by Warnken et al. (2007) had significant organic contributions from peat, and consequently possessed DOC contents (ca. 11–15 mg L^{-1}) that were 2–6 times higher than those of the cave waters studied here. The DOC content of agricultural and urban test solutions presented by Amery et al. (2010) in turn measured 19–144 mg L^{-1} DOC, clearly challenging direct comparisons with typical cave waters regarding kinetic parameters and their relationships with organic components. Thus, the studied cave waters possibly vary insufficiently in NOM quality and quantity for noticeable effects on complex kinetics to eventuate. This narrow range of DOM characteristics in cave waters may itself reflect discriminative processes that NOM in dripwater is subject to (*e.g.*, adsorption, filtration, or co-precipitation).

This notion is supported by CLE experiments performed on $CaCl_2$ soil extracts from three of the studied caves, which contained considerably higher metal and DOM concentrations than the waters (Table 1). These experiments yielded four adequate kinetic models (Fig. 3), while the remaining transition metal patterns precluded reliable model fits. Soil extracts were not augmented with elemental stock given their greater native elemental content compared to water samples. Despite this, only Cu consistently dissociated from M-NOM complexes during the experiments as evident in monotonous Cu uptake by Chelex-100. In soils from Hodge Creek Cave and Majumba Cave, both Ni and Co measurements were unreliable and varied incoherently over the course of 2 h, implying limited complex dissociation and/or re-association. These differences between Ni and Co compared to Cu are likely explained by the much higher native concentrations of Cu (ca. 4.2–7.0 μg L^{-1} compared to 0.1–0.3 μg L^{-1} and 0.9–2.8 μg L^{-1} for Co and Ni, respectively), translating to considerably higher M:DOC ratios for Cu that are predicted to result in increased lability of Cu. Compared to dripwater solutions, however, fitted distributions of $\ln(k_d)$ altogether indicated a larger stable fraction for Cu-NOM complexes (39–61 %). Similarly, 32–60 % of Ni and 80–91 % of Co remained complexed in soil extracts after 2 h, attesting to substantially greater Ni-NOM and Co-NOM stability than in any water sample. Indeed, relative to drip water solutions these stronger complexation regimes of soil extracts coincided with higher aromaticity, lower degrees of humification, as well as a greater fraction of fulvic acids as estimated by UV-spectral parameters (Fig. S1).

However, in this study, bounds of σ (Equation S5) were not adequately estimated by the log-normal model, yielding the unrealistically large distributions around μ. Fitted values of μ were in turn consistent with estimates from comparable environments (*e.g.*, 10^{-5} – 10^{-3} s^{-1} for Cu, Shi et al., 2016; order of 10^{-5} s^{-1} for Co in river water; Fasfous et al., 2004), suggesting that the excessive values of σ were in fact computational artefacts (cf. magnitude of $0.1 < \sigma < 2.2$ in Amery et al., 2010). As a compromise, k_d values were additionally approximated based on the conventional model depicted in Equation S4, which numerically reduces ligand action to a discrete number of binding sites. For most test solutions, the best fits were obtained when assuming either two or three kinetically distinguishable components (*i.e.*, fractions of distinct lability) (Table 2). In their magnitude, these estimates of the dominant component were generally in good agreement with those obtained for μ but were inconsistently related. Although discrepancies between the models are to be expected due to their distinct underlying assumptions, they also highlight the complexity of kinetic characterisations, as well as their high sensitivity to both method and data analysis (*e.g.*, Fasfous et al., 2004; Rose and Waite, 2003; Sigg et al., 2006). Solely based on fitted values of k_d, for instance, the CLE data implied that Ni was bound more weakly than Mg and Sr in several test solutions (Table 2; Table S1). In this example, the fitted dissociation rate constants do not account for the virtually complete removal of Mg and Sr from solution over the course of experiments (*i.e.*, effectively variable τ), whereas significant remnant undissociated Ni fractions and considerable 'inert' components of Ni in all solutions attest to stronger complexation.

Another caveat of this study relates to the heterogeneity in size of OMCs, and uncertainty around the contribution of different size fractions to the overall kinetic signatures. In this study, we opted to filter test solutions by 0.45 μm prior to the experiments in order to assess the

kinetic behaviour of OMCs in smaller colloids and nanoparticles. Previous efforts to constrain the role of different OM size fractions in cave systems suggest that during baseline flow conditions, metals are dominantly transported by these finer organic fractions (Hartland et al., 2011). The observed kinetic behaviour thus does not reflect that associated with larger particles, which tend to be mobilised and often included in speleothems during short-lived periods of high flow rates (Borsato et al., 2007; Warken et al., 2022). Within the <0.45 μm size fraction, however, we cannot distinguish the source or speciation of measured metals, nor can we account for potential re-equilibration of OMCs in the aliquots on the scale of seconds upon removal of Chelex-100 and before acidification. Further uncertainty arises from potential metal binding by the HEPES buffer (Mash et al., 2002), as well as from propagated errors in the added metal spike. The latter were estimated to result in up to 8 % deviations from the target 5 μg L^{-1}, adding to propagated analytical uncertainties in the quantification of metal concentrations. Albeit not readily quantifiable, these uncertainties are expected to contribute to some of the observed variability in the final kinetic parameters.

Given methodological and computational caveats encountered here, it may be necessary to adopt an alternative empirical approach to improve confidence in quantitative estimates of in-cave OMC decay kinetics. In this regard, diffusive gradients in thin-films (DGT) may present a feasible option to help circumvent analytical challenges related to low native metal concentrations, given their capacity to accumulate metals over time (*e.g.*, Sigg et al., 2006). A well-constrained DGT setup could potentially be deployed *in-situ* to allow for more representative characterisation of OMC decay (*e.g.*, Hartland et al., 2011). Nonetheless, the data obtained from CLE experiments provide insights into the heterogeneous nature of metal binding in cave waters with indicative quantifications that enable an assessment of potential implications for metal inclusion into speleothems.

4.2. OMC decay during speleothem formation

OMC decay is driven by the availability of a competitive sink for metal cations. In caves, such a sink is provided by calcium carbonate precipitating from infiltrating waters (Elzinga et al., 2006). The partitioning of Co in the absence of ligands (*i.e.*, under 'inorganic' experimental conditions) occurs with slight preference for the crystal phase (inorganic partition coefficient (k_p) for calcite ≈ 4), whereas even a small degree of carbonate precipitation would effectively remove most Cu from solution (k_p > 40) (Lindeman et al., 2022). While ligand action in natural systems is thus arguably essential for the presence of Cu in speleothems in measurable quantities, the underlying substantial control of prior carbonate precipitation (PCP; see *e.g.*, Fairchild and Treble, 2009) along the dripwater flow path complicates the use of Cu as a proxy based on OMC decay alone. Importantly, the susceptibility to PCP is less pronounced for Co, and negligible for Ni with an empirical k_p value of ca. 1 (Lindeman et al., 2022; Wang and Xu, 2001), indicating a largely indiscriminate incorporation of Ni in carbonate relative to Ca. Thus, the net measured distribution of these metals between water and associated carbonate precipitate in natural systems is expected to be foremost controlled by the dissociation of OMCs serving as the source of metals available for inclusion into carbonate.

The available metal fraction as a function of drip rate can be estimated based on the time-dependent decay of OMCs parameterised by μ and associated fit uncertainties (Fig. 4a). Across the range of empirical k_d values based on the log-normal model, the labile (taken to be 'available') metal fraction is most sensitive within time windows relevant for typical cave drip points (*i.e.*, <1–30 drips min^{-1}; Baker et al., 1997), although reaching an asymptote from ca. 40 drips min^{-1} (ca. 5.6 mL min^{-1}). At very high drip rates (*e.g.*, >60 drips min^{-1} or >8.4 mL min^{-1}), residence time is thus insufficient for OMC decay to contribute significantly to the labile metal pool, whereas the contribution increases exponentially towards longer drip intervals (*e.g.*, order of few drips per hour or day).

The modelled relationship of $[M]_{labile}$ with drip rate was most distinct for stable complexation regimes observed in CLE experiments, while test solutions with μ closer to 0 imply that OMC decay would be essentially indistinguishable from the dissociation of metal-aqua complexes (Amery et al., 2010). However, considering that the fitted uncertainties of μ used in the model were greatly exceeded by the range of values of k_d implied by the presumably mischaracterised (and hence ignored) distribution parameter σ, it is reasonable to assume that the metal supply by OMC decay is overall underestimated. Indeed, discrete

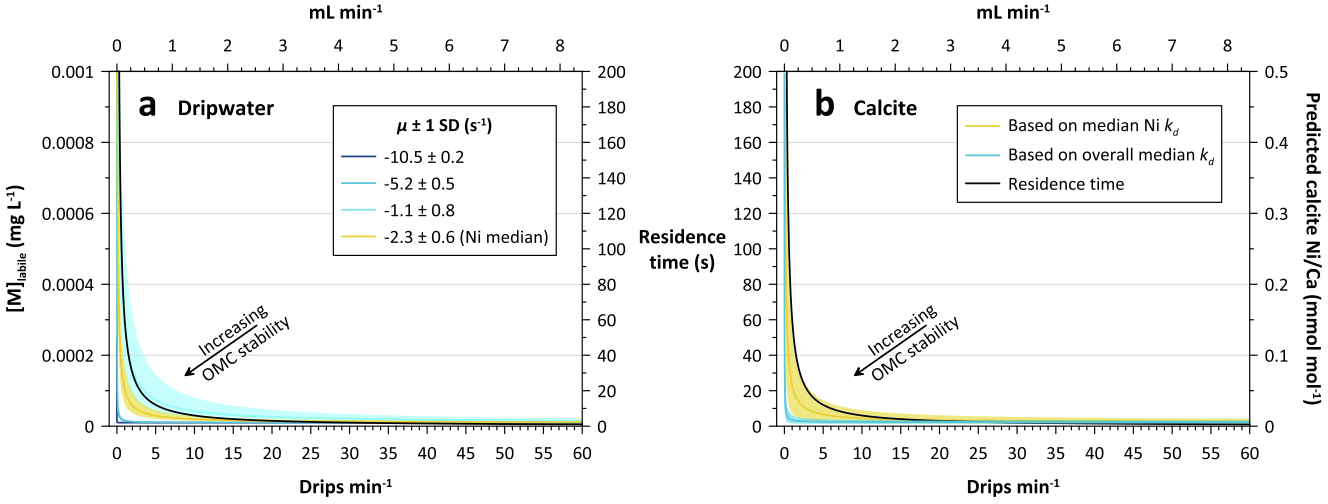

Fig. 4. Theoretical supply of labile metals to stalagmite surfaces as a function of drip rate and OMC decay. **a)** Simple forward model of metal release from OMCs at the dripwater-calcite interface based on empirical minimal, median, and maximal estimates of μ for transition metal datasets. Uncertainty envelopes denote the respective error margin (1 SD) of μ as determined by the fitting routine. **b)** Example prediction of theoretical Ni/Ca in a calcite stalagmite (orange line and shading) based on the empirical median $k_{d,\ Ni\text{-}NOM}$ shown in sub-figure **a** and assuming an inorganic partition coefficient of Ni into calcite of 1.1 ± 0.5 (Lindeman et al., 2022). The blue line and shaded area depict the same calculation but using the overall median k_d, reflecting higher overall OMC stability. Both parts of the model suggest a maximal sensitivity of OMC-driven metal supply for ca. <30 drips min^{-1} (<4.2 mL min^{-1}). The conversion of drip rate (bottom x-axes) to an approximate flow rate in mL min^{-1} (top x-axes) in both sub-figures assumes a single drop volume of 0.14 mL (e.g., Genty and Deflandre, 1998). Black solid lines in both sub-figures denote the approximate residence time as a function of drip rate, which approaches infinity with ceasing drips. Details on model assumptions and calculations are found in the Supplementary Material.

site models suggest substantially more stable kinetic components present in many samples to varying extent (Table 2), which would increasingly contribute to the labile metal pool at longer drip intervals. By example of Ni (using the median empirical estimate of $\mu \approx 2.3\ s^{-1}$) and assuming a realistic aqueous Ni/Ca (here, 0.01 mmol mol^{-1}), the model can be extended to make a simplistic prediction of the impact on calcite Ni/Ca as a function of drip interval (Fig. 4b).

Using an inorganic partition coefficient of Ni of 1.1 (Lindeman et al., 2022) with a conservative uncertainty of ±0.5, and accepting negligible influence of other processes on partitioning, the same initial data support that metal supply to stalagmite tips through OMC decay likely occurs on relevant time-scales and across measurable magnitudes. By extension, these findings thus imply that under favourable circumstances (*i.e.*, OMC decay dominates metal supply), the concentration of Ni and potentially other transition metals may indeed allow for reconstructions of dripwater residence times, and ultimately flow rates. Where complex stability is very high, however, OMC decay may occur at insufficient rates and only imprint on carbonate M/Ca at very long drip intervals. In this regard, however, the variability in k_d observed between samples and metals in both continuous and discrete kinetic models illustrates that empirical estimates are not sufficiently constrained or generalisable for reliable quantitative models. To achieve the latter, system-specific calibration of kinetic parameters through cave monitoring may be required to inform an appropriate distribution of k_d. Moreover, a practical use of the model would further require a systematic approach to evaluate the relative contribution of both the OMC decay and direct inclusion of OMCs to the final measured metal concentration in the speleothem fabric, including practical criteria to distinguish between both metal delivery pathways. This could, for instance, be achieved with high-resolution microscopic techniques to elucidate the spatial distribution and nature of organic inclusions within speleothems (*e.g.*, Borsato et al., 2007), coupled with statistically-based criteria, and warranting a better understanding of the potentially complex site-specific dynamics of sources and transfer of organics in the dripwater (*e.g.*, Endres et al., 2023).

Regardless, our data at large support two key notions for the interpretation of trace element concentrations in dripwaters and speleothems. Firstly, we corroborate that binding of transition metals by organic ligands is universal to dripwaters and thus presents a critical rate-dependent control for the distribution of affected cations between aqueous and crystal phases. Subject to further characterisation, the latter may be quantified to link speleothem transition metal concentrations with dripwater residence time on stalagmite vertices, during which metals dissociate from the 'aqueous sink' and are captured by the 'carbonate sink' as conceptualised in Hartland and Zitoun (2018). Based solely on the kinetic signatures derived here, empirical estimates of $k_{d,\ Ni\text{-}NOM}$ suggest a resolvable release of labile Ni for <40 drips min^{-1} (<5.6 mL min^{-1}), which is predicted to be imprinted in calcite Ni/Ca measurements. In absence of detrital contamination, (*e.g.*, due to flushing events that mobilise larger colloidal or particulate fractions (operationally excluded here) and cause local metal accumulations in the speleothem fabric), we argue that OMC equilibrium kinetics may thus present a major driver of the net inclusion of similarly behaving first-row transition metals and possibly some rare earth elements (Sliwinski et al., 2022). Secondly, the experiments illustrate the effective absence of kinetic limitation by ligands on alkaline earth metals such as Mg and Sr, arguing for their more straightforward inclusion pathway from dripwater to speleothems. This observation in turn supports the use of different elemental signatures as mechanistically distinct and complementary proxies, which can greatly enhance interpretive power of speleothem trace element datasets.

5. Conclusions

Organic complexation pervasively governs the speciation of many trace metals in cave dripwaters, imparting kinetic constraints on their availability to speleothems. Competitive ligand exchange experiments performed in this study demonstrate considerable variability in OMC decay kinetics between transition metals in natural dripwaters and soil extracts, depicting a hierarchy of OMC stability of Cu ≈ Co > Ni ≫ Mg, Sr. However, in absence of distinct covariation between derived OMC dissociation rate constants with proxies of NOM properties, the variability of dripwater OMC decay rates was largely unpredictable. The ambiguity of controlling factors of kinetic signatures was exacerbated by a problematic model description of log-normal distributions of k_d as implemented herein. However, additional discrete site models provided further confidence, depicting a range of site stabilities with considerable 'inert' fractions for transition metals, and lack of the latter for Mg and Sr. Although these findings emphasise a pronounced sensitivity of kinetic properties to methodology, empirical parameters suggested favourable kinetic time-scales of OMC decay to potentially dominate metal supply to speleothems at drip rates commonly found in caves (<1 to ca. 40 drips min^{-1}, or up to ca. 5.6 mL min^{-1}). With precedent provided by Lindeman et al. (2022), this observation in turn raises the question whether kinetic signals could be reliably distinguished in calcite deposits, which requires experimental investigation into OMC decay kinetics and metal inclusion into calcite analogous of stalagmite growth.

Data availability

Data are available through Mendeley Data at https://doi.org/10.17632/5xyxgzm4hp.2.

CRediT authorship contribution statement

Sebastian N. Höpker: Conceptualization, Data curation, Formal analysis, Methodology, Visualization, Writing – original draft, Writing – review & editing. **Sebastian F.M. Breitenbach:** Conceptualization, Funding acquisition, Writing – review & editing. **Megan Grainger:** Conceptualization, Methodology, Supervision, Writing – review & editing. **Claudine H. Stirling:** Formal analysis, Methodology, Writing – review & editing, Resources. **Adam Hartland:** Conceptualization, Funding acquisition, Methodology, Resources, Supervision, Writing – review & editing.

Declaration of competing interest

The authors declare that they have no known competing financial interests or personal relationships that could have appeared to influence the work reported in this paper.

Acknowledgements

The research was funded by the Royal Society Te Apārangi Rutherford Discovery Fellowship programme (grant no. RDF-UOW1601), the European Union's Horizon 2020 Research and Innovation programme through a Marie Skłodowska-Curie grant (grant no. 691037), and the Ministry of Business, Innovation and Employment through a Smart Ideas grant (grant no. UOWX2102). The authors thank Travis Cross, Jeffrey Lang, Christopher Wood, Andrew Pearson, and Jessica Höpker for help with fieldwork. We also thank Andrew Rate and Peter Reutemann for helpful discussions. We are grateful for sampling permissions granted by the Department of Conservation, James Glenn, Darden King, and the Pōhaturoa Trust. We thank Mélanie Davranche for editorial handling of our manuscript, and Jakub Sliwinski and one anonymous reviewer for helpful comments upon our first submission.

Appendix A. Supplementary material

The Supplementary Material contains supporting data presented in Table S1 (derived kinetic characteristics of Mg and Sr), Table S2 (basic information on sampling locations), and Fig. S1 (selected relationships

between derived kinetic and organic indices), as well as detailed information on methodology and analytical techniques applied in this study. Tables S1 and S2 are also provided in spreadsheet form. Supplementary Material to this article can be found online at https://doi.org/10.1016/j.gca.2024.03.024.

References

Allen, H.B., Hansen, D.J., 1996. The importance of trace metal speciation to water quality criteria. Water Environ. Res. 68, 42–54.

Amery, F., Degryse, F., Moorleghem, C.V., Duyck, M., Smolders, E., 2010. The dissociation kinetics of Cu-dissolved organic matter complexes from soil and soil amendments. Anal. Chim. Acta. 670, 24–32.

Artinger, R., Buckau, G., Geyer, S., Fritz, P., Wolf, M., Kim, J.I., 2000. Characterization of groundwater humic substances: influence of sedimentary organic carbon. Appl. Geochem. 15, 97–116.

Baken, S., Degryse, F., Verheyen, L., Merckx, R., Smolders, E., 2011. Metal complexation properties of freshwater dissolved organic matter are explained by its aromaticity and by anthropogenic ligands. Environ. Sci. Technol. 45, 2584–2590.

Baker, A., Barnes, W.L., Smart, P.L., 1997. Variations in the discharge and organic matter content of stalagmite drip waters in Lower Cave, Bristol. Hydrol. Process. 11, 1541–1555.

Baker, A., Tipping, E., Thacker, S.A., Gondar, D., 2008. Relating dissolved organic matter fluorescence and functional properties. Chemosphere 73, 1765–1772.

Borsato, A., Frisia, A., Fairchild, I.J., Somogyi, A., Susini, A., 2007. Trace element distribution in annual stalagmite laminae mapped by micrometer-resolution x-ray fluorescence: implications for incorporation of environmentally significant species. Geochim. Cosmochim. Acta 71, 1494–1512.

Buffle, J., Wilkinson, K.J., Stoll, S., Filella, M., Zhang, J., 1998. A generalized description of aquatic colloidal interactions: the three-colloidal component approach. Environ. Sci. Technol. 32, 2887–2899.

Chakrabarti, C.L., Lu, Y., Gregoire, D.C., Back, M.H., Schroeder, W.H., 1994. Kinetic studies of metal speciation using chelex cation exchange resin: application to cadmium, copper, and lead speciation in river water and snow. Environ. Sci. Technol. 28, 1957–1967.

Collins, R.N., Kinsela, A.S., 2010. The aqueous phase speciation and chemistry of cobalt in terrestrial environments. Chemosphere 79, 763–771.

Doucet, F.J., Lead, J.R., Santschi, P.H., 2007. Colloid–trace element interactions in aquatic systems. In: Wilkinson, K., Lead, J.R. (Eds.), Environmental Colloids and Particles: Behaviour, Separation and Characterisation. John Wiley and Sons Ltd., Chichester, UK, pp. 95–157.

Elzinga, E.J., Rouff, A.A., Reeder, R.J., 2006. The long-term fate of Cu2+, Zn2+, and Pb2 + adsorption complexes at the calcite surface: an X-ray absorption spectroscopy study. Geochim. Cosmochim. Acta 70, 2715–2725.

Endres, L.S., Jacquin, C., González-Lemos, S., Rodríguez-Rodríguez, L., Sliwinski, J., Kaushal, N., Kost, O., Stoll, H.M., 2023. Climatic and cave settings influence on drip water fluorescent organic matter with implications for fluorescent laminations in stalagmites. Quat. Res. 1–21.

Fairchild, I.J., Treble, P.C., 2009. Trace elements in speleothems as recorders of environmental change. Quat. Sci. Rev. 28, 449–468.

Fasfous, I.I., Yapici, T., Murimboh, J., Hassan, N.M., Chakrabarti, C.L., Back, M.H., Grégoire, D.C., 2004. Kinetics of trace metal competition in the freshwater environment: some fundamental characteristics. Environ. Sci. Technol. 38, 4979–4986.

Filella, M., Buffle, J., 1993. Factors controlling the stability of submicron colloids in natural-waters. Colloids Surf. A 73, 255–273.

Genty, D., Deflandre, G., 1998. Drip flow variations under a stalactite of the Père Noël cave (Belgium). Evidence of seasonal variations and air pressure constraints. J. Hydrol. 211, 208–232.

Hartland, A., Zitoun, R., 2018. Transition metal availability to speleothems controlled by organic binding ligands. Geochem. Perspect. Lett. 22–25.

Hartland, A., Fairchild, I.J., Lead, J.R., Zhang, H., Baalousha, M., 2011. Size, speciation and lability of NOM–metal complexes in hyperalkaline cave dripwater. Geochim. Cosmochim. Acta 75, 7533–7551.

Hartland, A., Fairchild, I.J., Lead, J.R., Borsato, A., Baker, A., Frisia, S., Baalousha, M., 2012. From soil to cave: transport of trace metals by natural organic matter in karst dripwaters. Chem. Geol. 304, 68–82.

Hoffmann, S.R., Shafer, M.M., Armstrong, D.E., 2007. Strong colloidal and dissolved organic ligands binding copper and zinc in rivers. Environ. Sci. Technol. 41, 6996–7002.

Huang, Y., Fairchild, I.J., 2001. Partitioning of Sr^{2+} and Mg^{2+} into calcite under karst-analogue experimental conditions. Geochim. Cosmochim. Acta 65, 47–62.

Irving, H., Williams, R.J., 1953. The stability of transition-metal complexes. J. Chem. Soc. 3192 (Resumed).

Lam, M.T., Murimboh, J., Hassan, N.M., Chakrabarti, C.L., 1999. Competitive ligand exchange/adsorptive cathodic stripping voltammetry (CLE/AdCSV) for kinetic studies of nickel speciation in aqueous environmental samples containing heterogeneous, macromolecular, organic complexants. Anal. Chim. Acta. 402, 195–209.

Lead, J.R., Wilkinson, K.J., 2006. Aquatic colloids and nanoparticles: current knowledge and future trends. Environ. Chem. 3, 159.

Levy, J.L., Zhang, H., Davison, W., Puy, J., Galceran, J., 2012. Assessment of trace metal binding kinetics in the resin phase of diffusive gradients in thin films. Anal. Chim. Acta. 717, 143–150.

Lindeman, I., Hansen, M., Scholz, D., Breitenbach, S.F., Hartland, A., 2022. Effects of organic matter complexation on partitioning of transition metals into calcite: cave-analogue crystal growth experiments. Geochim. Cosmochim. Acta 317, 118–137.

Mandal, R., Sekaly, A.L., Murimboh, J., Hassan, N.M., Chakrabarti, C.L., Back, M.H., Schroeder, W.H., 1999. Effect of the competition of copper and cobalt on the lability of Ni(II)–organic ligand complexes, Part II: in freshwaters (Rideau River surface waters). Anal. Chim. Acta. 395, 323–334.

Mash, H.E., Chin, Y.-P., Sigg, L., Hari, R., Xue, H., 2002. Complexation of copper by zwitterionic aminosulfonic (Good) buffers. Anal. Chem. 75, 671–677.

Miller, C.L., Liang, L., Gu, B., 2012. Competitive ligand exchange reveals time dependant changes in the reactivity of Hg–dissolved organic matter complexes. Environ. Chem. 9, 495–501.

Rate, A.W., McLaren, R.G., Swift, R.S., 1992. Evaluation of log-normal distribution first-order kinetic model for copper(II)-humic acid complex dissociation. Environ. Sci. Technol. 26, 2477–2483.

Rate, A.W., McLaren, R.G., Swift, R.S., 1993. Response of copper(II)-humic acid dissociation kinetics to factors influencing complex stability and macromolecular conformation. Environ. Sci. Technol. 27, 1408–1414.

Rieuwerts, J.S., Thornton, I., Farago, M.E., Ashmore, M.R., 1998. Factors influencing metal bioavailability in soils: preliminary investigations for the development of a critical loads approach for metals. Chem. Speciation Bioavail. 10, 61–75.

Rose, A.L., Waite, T.D., 2003. Kinetics of iron complexation by dissolved natural organic matter in coastal waters. Mar. Chem. 84, 85–103.

Sanders, J.R., Bloomfield, C., 1980. The influence of pH, ionic strength and reactant concentrations on copper complexing by humified organic matter. J. Soil Sci. 31, 53–63.

Shafaei Arvajeh, M.R., Lehto, N., Garmo, Ø.A., Zhang, H., 2013. Kinetic studies of Ni organic complexes using diffusive gradients in thin films (DGT) with double binding layers and a dynamic numerical model. Environ. Sci. Technol. 47, 463–470.

Shi, Z., Wang, P., Peng, L., Lin, Z., Dang, Z., 2016. Kinetics of heavy metal dissociation from natural organic matter: roles of the carboxylic and phenolic sites. Environ. Sci. Technol. 50, 10476–10484.

Sigg, L., Behra, R., 2005. Metal Ions in Biological Systems. CRC Press.

Sigg, L., Black, F., Buffle, J., Cao, J., Cleven, R., Davison, W., Zhang, H., 2006. Comparison of analytical techniques for dynamic trace metal speciation in natural freshwaters. Environ. Sci. Technol. 40, 1934–1941.

Sliwinski, J.T., Kost, O., Endres, L., Iglesias, M., Haghipour, N., González-Lemos, S., Stoll, H.M., 2022. Exploring soluble and colloidally transported trace elements in stalagmites: the strontium-yttrium connection. Geochim. Cosmochim. Acta 343, 64–83.

Wang, Y., Xu, H., 2001. Prediction of trace metal partitioning between minerals and aqueous solutions: a linear free energy correlation approach. Geochim. Cosmochim. Acta 65, 1529–1543.

Warken, S.F., Kuchalski, L., Schröder-Ritzrau, A., Vieten, R., Schmidt, M., Höpker, S.N., Hartland, A., Spötl, C., Scholz, D., Frank, N., 2022. The impact of seasonal and event-based infiltration on transition metals (Cu, Ni, Co) in tropical cave drip water. Rapid Commun. Mass Spectrom. 36, e9278.

Warnken, K.W., Davison, W., Zhang, H., Galceran, J., Puy, J., 2007. Measurements of metal complex exchange kinetics in freshwater. Environ. Sci. Technol. 41, 3179–3185.

Wassenburg, J.A., Riechelmann, S., Schröder-Ritzrau, A., Riechelmann, D.F., Richter, D. K., Immenhauser, A., Scholz, D., 2020. Calcite Mg and Sr partition coefficients in cave environments: Implications for interpreting prior calcite precipitation in speleothems. Geochim. Cosmochim. Acta 269, 581–596.

Welikala, D., Hucker, C., Hartland, A., Robinson, B.H., Lehto, N.J., 2018. Trace metal mobilization by organic soil amendments: insights gained from analyses of solid and solution phase complexation of cadmium, nickel and zinc. Chemosphere 199, 684–693.

Xue, H.B., Jansen, S., Prasch, A., Sigg, L., 2000. Nickel speciation and complexation kinetics in freshwater by ligand exchange and DPCSV. Environ. Sci. Technol. 35, 539–546.